Geophysical Research Letters

RESEARCH LETTER
10.1029/2022GL099953

Coseismic Folding During Ramp Failure at the Front of the Sulaiman Fold-and-Thrust Belt

Muhammad Tahir Javed[1], Sylvain Barbot[2], Farhan Javed[3], Aamir Ali[4], and Carla Braitenberg[1]

[1]Department of Mathematics and Geosciences, University of Trieste, Trieste, Italy, [2]Department of Earth Sciences, University of Southern California, Los Angeles, CA, USA, [3]Centre for Earthquake Studies, National Centre for Physics, Islamabad, Pakistan, [4]Department of Earth Sciences, Quaid-i-Azam University, Islamabad, Pakistan

Key Points:

- 2015 Mw 5.7 Dajal, Pakistan earthquake ruptured the blind front of the Sulaiman Fold Thrust belt
- Coseismic deformation includes slip on a blind thrust and flexural slip in the hanging wall
- The buried section of the Boundary Thrust extends 30 km farther south of the fault trace

Supporting Information:

Supporting Information may be found in the online version of this article.

Correspondence to:

M. T. Javed,
muhammadtahir.javed@phd.units.it

Citation:

Javed, M. T., Barbot, S., Javed, F., Ali, A., & Braitenberg, C. (2022). Coseismic folding during ramp failure at the front of the Sulaiman fold-and-thrust belt. *Geophysical Research Letters*, *49*, e2022GL099953. https://doi.org/10.1029/2022GL099953

Received 7 JUN 2022
Accepted 13 NOV 2022

Author Contributions:

Conceptualization: Muhammad Tahir Javed, Sylvain Barbot, Farhan Javed, Aamir Ali
Data curation: Muhammad Tahir Javed, Farhan Javed
Formal analysis: Muhammad Tahir Javed, Sylvain Barbot, Farhan Javed, Aamir Ali, Carla Braitenberg
Funding acquisition: Sylvain Barbot, Carla Braitenberg
Investigation: Muhammad Tahir Javed, Sylvain Barbot, Farhan Javed, Aamir Ali, Carla Braitenberg
Methodology: Muhammad Tahir Javed, Sylvain Barbot, Farhan Javed
Project Administration: Sylvain Barbot, Carla Braitenberg
Resources: Aamir Ali, Carla Braitenberg

Abstract The Sulaiman Fold Thrust (SFT) in Central Pakistan formed during the India-Eurasia collision in the late Cenozoic. However, the mechanics of shortening of the brittle crust at time scales of seismic cycles is still poorly understood. Here, we use radar interferometry to analyze the deformation associated with the 2015 magnitude (Mw) 5.7 Dajal blind earthquake at the eastern boundary of the SFT. We use kinematic inversions to determine the distribution of slip on the frontal ramp and of flexural slip along active axial surfaces for the forward- and backward-verging two end-member models: a double fault-bend-fold system and a fault-propagation-fold. In both models, a décollement branches into a shallow ramp at approximately 7.5 km depth with coseismic folding in the hanging wall. The Dajal earthquake ruptured the base of the Boundary Thrust buried under the sediment from the Indus-River floodplain, representing fault-bend or fault-propagation folding some 30 km off its nearest surface exposure.

Plain Language Summary The relative motion between tectonic plates is accommodated across wide fault zones that concentrate deformation. Yet, how these deformation zones grow over time is poorly known. In this study, we investigate the Sulaiman Fold-Thrust (SFT) belt, Pakistan at the plate boundary between the Indian and Eurasian continents. We use radar interferometry to estimate the crustal deformation induced by the 2015 Mw 5.7 Dajal earthquake at the eastern margin of the SFT. The rupture did not reach the surface at the eastern extension of the SFT, buried under the younger sediments of the Indus River floodplain. The rupture and associated folding in the hanging wall documents the eastward growth of the SFT. These observations document the seismic potential of hidden ramps in fold-and-thrust belts and the control on final rupture size by fault-bends and surrounding folds.

1. Introduction

The kinematics of crustal deformation at fold-and-thrust belts is complicated by the interaction between faulting and folding (Chapple, 1978; Muñoz & Charrier, 1996; Nabavi & Fossen, 2021; Poblet & Lisle, 2011; Price, 1981; Sepehr & Cosgrove, 2004). Complex fault geometry causes shortening in the hanging wall that is accommodated by flexural slip, a type of plastic deformation that results from slip on multiple bedding planes in sedimentary strata (Couples et al., 1998; Johnson, 2018; Johnson & Johnson, 2002; Kaneko et al., 2015; Sathiakumar et al., 2020; Suppe, 1983; Tanner, 1989). Subduction zones exhibit a thrust-and-fold belt in the forearc near the trench (D. Davis et al., 1983; Kopp & Kukowski, 2003; Saffer & Bekins, 2002; Qiu & Barbot, 2022), even in the poorly developed frontal prism of erosive margins (e.g., Eakin et al., 2014; Tsuji et al., 2011; Von Huene et al., 1985). Thrust-and-fold belts can also be found at the margin of collision zones (Hubbard et al., 2015, 2016; Lavé & Avouac, 2000; Yue et al., 2005) and in other transpressive settings (Lai et al., 2006; Namson & Davis, 1988; Shaw & Shearer, 1999; Shaw & Suppe, 1994, 1996; Shaw et al., 2004; Tapponnier et al., 1990). The role of folding on the long-term build-up of topography is well explained in various tectonic environments (T. L. Davis et al., 1989; Kastelic & Carafa, 2012; Mahanjane & Franke, 2014; Shaw et al., 2005). However, the mechanical coupling between folding and faulting during seismic cycles is still poorly understood. Some observations (J. Lin & Stein, 1989; A. Lin et al., 2001; Kuo et al., 2014) and numerical modeling (Sathiakumar et al., 2020) indicate that co-seismic folding is possible, but how this deformation occurs in the crust is still poorly resolved.

The relative convergence between the Indian subcontinent and the Afghan block results in underthrusting of the Indian plate (inset Figure 1a). The western margin of the India-Eurasia collision belt, which accommodates around half of 35–46 mm/yr of relative plate motion (Ul-Hadi et al., 2013), provides an ideal setting to study

Software: Muhammad Tahir Javed, Farhan Javed
Supervision: Sylvain Barbot, Carla Braitenberg
Validation: Muhammad Tahir Javed, Sylvain Barbot, Farhan Javed, Aamir Ali, Carla Braitenberg
Visualization: Muhammad Tahir Javed, Farhan Javed, Aamir Ali, Carla Braitenberg
Writing – original draft: Muhammad Tahir Javed
Writing – review & editing: Muhammad Tahir Javed, Sylvain Barbot, Farhan Javed, Aamir Ali, Carla Braitenberg

the mechanics of an active fold-and-thrust belt (Figure 1a) (Banks & Warburton, 1986). The shear component is accommodated along the transform boundary of the Chaman Fault (CF) system but shortening is taken up by the transpressive Kirthar Fold Thrust and the Sulaiman Fold Thrust (SFT) (Bernard et al., 2000; Fattahi & Amelung, 2016; Saif-Ur-Rehman et al., 2020; Szeliga et al., 2012). The deformation front separating Eurasia from the Indian subcontinent in Central Pakistan is the Boundary Thrust (BT), at the eastern limit of the SFT. The SFT belt is seismically active with many devastating earthquakes occurring within a complex network of blind thrusts, fault bends, duplex structures, and strike-slip faults (Banks & Warburton, 1986; Jadoon, 1995; Prevot et al., 1980). The historical earthquakes and fault plane solutions in the SFT belt in the last three decades are shown in Figure 1a. The regional seismicity is characterized by thrust and a few strike-slip earthquakes (Pezzo et al., 2014; Reynolds et al., 2015). For example, the doublet thrust of Mw 6.9 events that occurred on 27 February 1997, separated by approximately 19 s, caused many fatalities and major economic loss (Nissen et al., 2016). Although the Central and Western SFT are characterized by well-developed fault-bend folding structures, the structures in the eastern SFT zones are under-developed (Banks & Warburton, 1986; Khan & Scarselli, 2021; Saif-Ur-Rehman et al., 2019), experiencing only moderate-size NorthEast-SouthWest and E-W thrust earthquakes, with a deficit of large (Mw > 6.0) earthquakes along the BT in the last several decades. Large cities with population of more than 3 million are located approximately 10–50 km from the BT (Figure 1a).

On 23 October 2015, a Mw 5.7 earthquake occurred near Dajal, 55 km South-SouthWest of Dera Ghazi Khan, one of the most populated cities of Punjab province, Pakistan (Figure 1a). The earthquake occurred at the eastern boundary of the SFT, providing an opportunity to study the interaction of coseismic slip and folding within an active fold-and-thrust belt (Figures 1b and 1c). Here, we investigate the deformation induced by the 2015 Mw 5.7 Dajal earthquake to gain new insights into the mechanics of folding through flexural slip during the seismic cycle. The orientation and maturity of the frontal fold-and-thrust belt is still poorly understood. A preliminary geological interpretation of a controlled-source seismic profile across the BT some 20–30 km north of the epicenter infers the presence of a shallow thrust, dipping eastwards at an angle of 30°–40°, possibly rooted in a décollement at 5–10 km depth forming a double fault-bend fold (FBF) or a fault-propagation fold (FPF) system (Humayon et al., 1991; Saif-Ur-Rehman et al., 2019). The double FBF system is defined by two horizontal décollements separated by a frontal ramp and associated active axial surfaces originating at the fault bends (Suppe, 1983), whereas the FPF system involves a deeper horizontal décollement and the frontal ramp that terminates below a thick sediment layer along with their associated axial surfaces initiated at the fault bends and top of the fold (Sathiakumar et al., 2020; Suppe, 1983; Suppe & Medwedeff, 1990). A more recent interpretation of the controlled-source seismic profiles at the Eastern SFT zone in addition to the other geological and field observations invokes a FBF system with a pair of forward- and backward-verging faults (Humayon et al., 1991; Saif-Ur-Rehman et al., 2019).

Considering the uncertainties in fault orientation, we present kinematic inversions of interferometric synthetic aperture radar (InSAR) for two end-member models of coseismic folding that imply different stages of development of the frontal section: a double synclinal and anticlinal FBF system (Suppe, 1983) and a FPF system (Suppe & Medwedeff, 1990) (Figure 2). In addition, we consider either a forward-vergent (dipping westward), or a backward-vergent (dipping eastward) thrust. We take folding in the hanging wall into account explicitly by inverting for the spatial distribution of flexural slip along the active axial surfaces. In the FBF model with a backward-vergent thrust, considerable movement occurs on the west-dipping axial surfaces, which is physically implausible (Figure 3c). In the forward-vergent cases, flexural slip accumulates above the hinge of the ramp-décollement system (Figures 3a and 3b), with an amplitude compatible with predictions from balanced cross-sections for long-term deformation (Sathiakumar et al., 2020). Our observations show that folding occurred either during the earthquake rupture or during the short post-seismic phase that followed, which is also captured by the InSAR data. The 2015 Mw 5.7 Dajal earthquake was presumably confined within the blind ramp of the FPF or of the FBF system representing the frontal extension of the BT, where it is buried under the Miocene or younger sediment of the Indus River floodplain. These observations document the seismic potential of blind ramps and axial surfaces in fold-and-thrust belts and the control on final rupture size by fault-bends and surrounding folds.

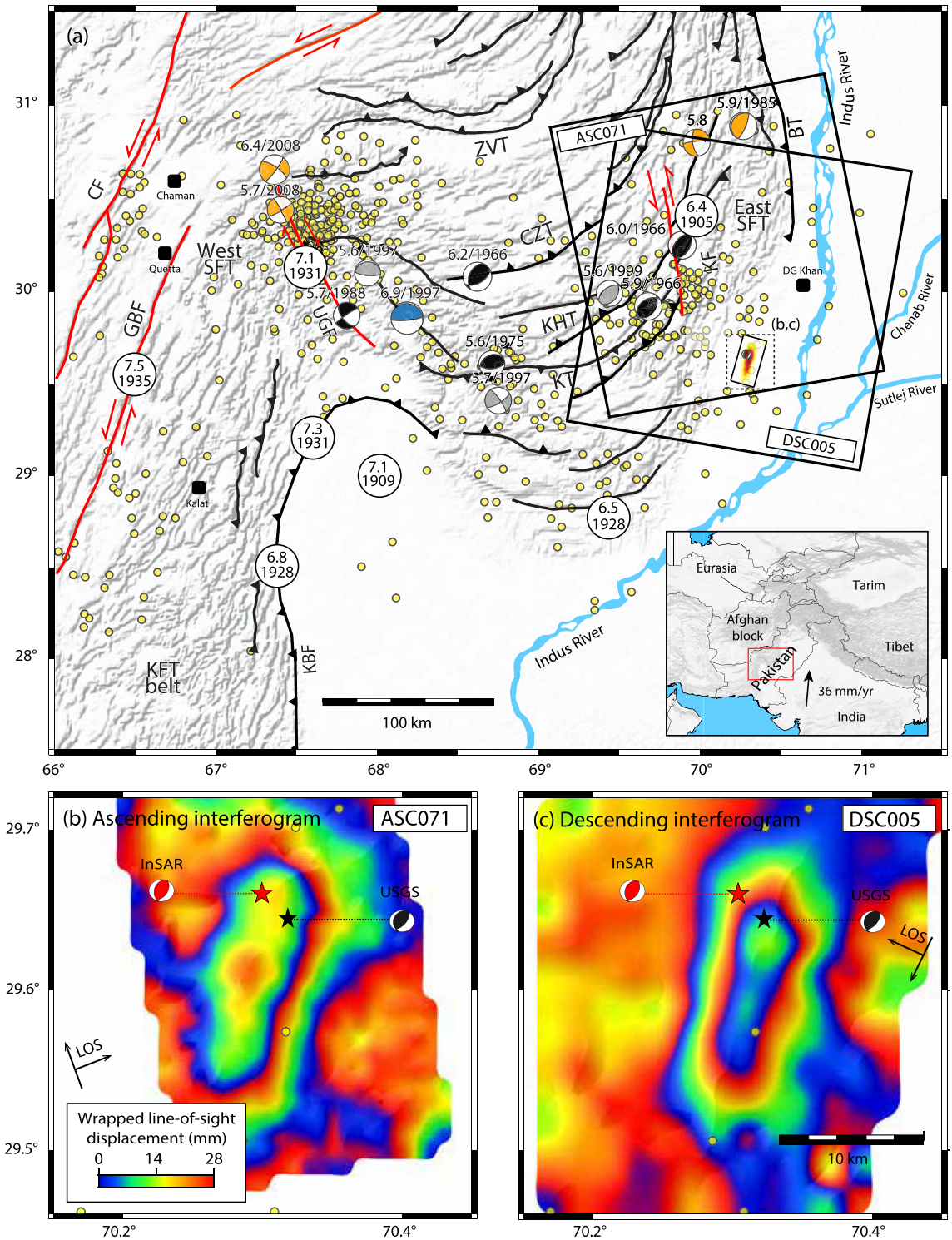

Figure 1. Tectonic settings and historical earthquakes (yellow circles) with $M > 3.5$ on Sulaiman Fold Thrust (SFT) belt. (a) Faults abbreviated with BT, boundary thrust, CF, Chaman Fault, GBF, Ghazaband Fault, KF, Kingri Fault, KT, Kamari Thrust, KHT, Karahi Thrust (Pezzo et al., 2014). Focal mechanism solutions in blue (Nissen et al., 2016), orange (Pezzo et al., 2014), Global Centroid Moment Tensor catalog, dark gray (Reynolds et al., 2015), black (Bernard et al., 2000), and white circles (Ambraseys & Bilham, 2003). The dark red moment tensor is the 2015 Dajal earthquake epicenter, shown above the slip distribution. The inset shows the geographical location of the SFT belt and the relative motion (36 mm/yr) between the India and the Afghan block (Ul-Hadi et al., 2013). (b and c) Ascending and descending, wrapped line-of-sight (LOS) displacement of the 2015 Dajal earthquake.

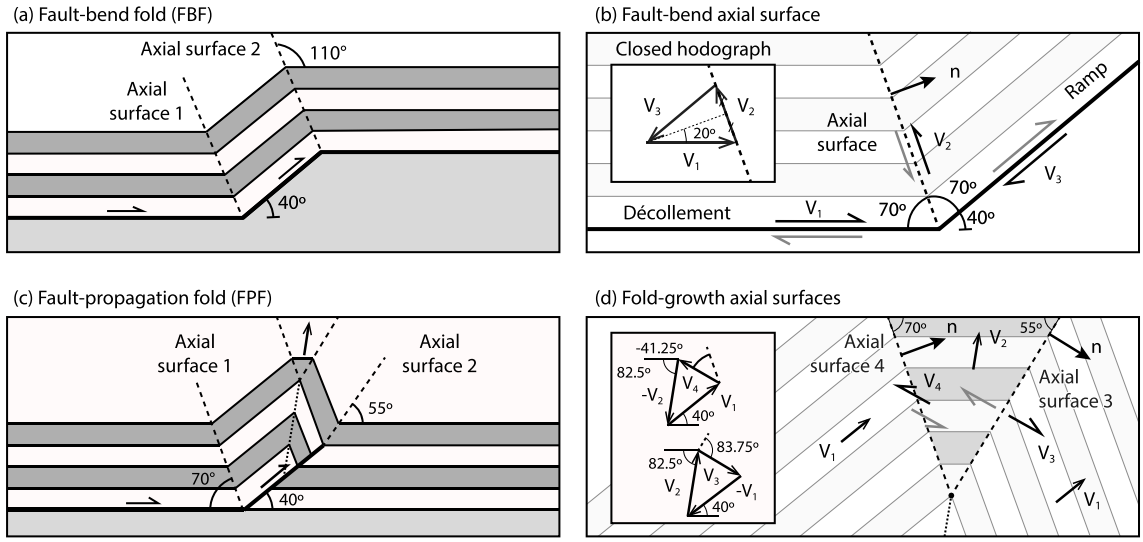

Figure 2. End-member models of fault-related folds in a representative cross-section. (a) Double fault-bend fold (FBF) model with syncline and anticlinal fault bends and active axial surfaces. (b) Long-term slip directions along the décollement, ramp, and axial surfaces. The three velocity vectors close the hodograph (inset). Flexural slip on axial surfaces accommodates the advection of thrusted sediments as they start or stop climbing the ramp. The unit vector **n** is normal to the axial surface. (c) FPF with four active axial surfaces (long dashed lines). The domains surrounded by active axial surface move at the same long-term velocity. The passive axial surface (short dashed line) does not contribute to internal deformation. (d) Relative motion along the top axial surfaces 3 and 4 of the fault-propagation fault model closing the hodographs (inset). The end-member models are extruded along a 194° strike to form a three-dimensional structure for the purpose of inversion.

2. Kinematic Inversion of Coseismic Slip and Folding

The 2015 Mw 5.7 Dajal earthquake occurred in a remote location, outside of any ground-based geodetic observatory. Fortunately, the deformation was captured by the spaceborne synthetic aperture radar (SAR) Sentinel-1A. To document the surface deformation induced by the earthquake, we generate the Sentinel-1A ascending (ASC071) and descending (DSC005) interferograms (Figures 1b and 1c), allowing us to constrain two directions of deformation. The ascending radar images were acquired on 17 October and 10 November; the descending images on 1 October and 18 November 2015, capturing 18 and 26 days of potential postseismic deformation in addition to the co-seismic deformation. For radar image formation and post-processing, we use GMT5SAR (Sandwell et al., 2011) (Section 1.1 in Supporting Information S1). We determine the uncertainties in the SAR interferograms based on the semi-variogram (Figure S3 in Supporting Information S1) (Section 1.2 in Supporting Information S1). The ascending and descending interferograms show line-of-sight displacements of approximately 45 and 50 mm, respectively (Figure S4 in Supporting Information S1). In a preliminary step, we estimate the simplified source parameters assuming coseismic rupture on a single fault plane, ignoring potential folding in the hanging wall. We constrain the dip, strike, depth, width, length, rake, and slip (Figure S6, Table S3 in Supporting Information S1) based on data from both interferograms using a Monte Carlo method for a rectangular patch of uniform slip (Bagnardi & Hooper, 2018) (Section 1.3 in Supporting Information S1). The seismic moment $M_0 = 3.94 \times 10^{17}$ N m, assuming a shear modulus of 32 GPa, is calculated using the mean value of the probability distribution of the source model parameters, corresponding to Mw 5.7. The epicentral location and source properties are similar to inferences from the U.S. Geological Survey (USGS, 2020), and the International Seismological Center (Lentas et al., 2019) (Table S3 in Supporting Information S1). The depth of 6.5 ± 1.2 km is similar to past events in the Eastern SFT region (Reynolds et al., 2015). This simple model indicates that the rupture took place on a 40° ± 12°-dipping thrust with strike 194° ± 6°, located east of the exposed SFT, buried deep below the Miocene or younger sediment of the Indus River floodplain. We use this result to construct a three-dimensional model of coseismic deformation compatible with the regional tectonic setting.

Based on the fold-and-thrust tectonic environment, we investigate forward- and backward-vergent thrusts for two relevant end-members of fault-bend geometries of crustal deformation that involve fault slip at the base of the thrust sheet and folding in the overlying sedimentary strata. In all cases, we surmise that a blind extension of the BT extends toward the Dajal earthquake epicentral area. In the FBF model, we consider slip on the décollement-ramp-décollement, and flexural slip along two active axial surfaces initiated at the fault-bends

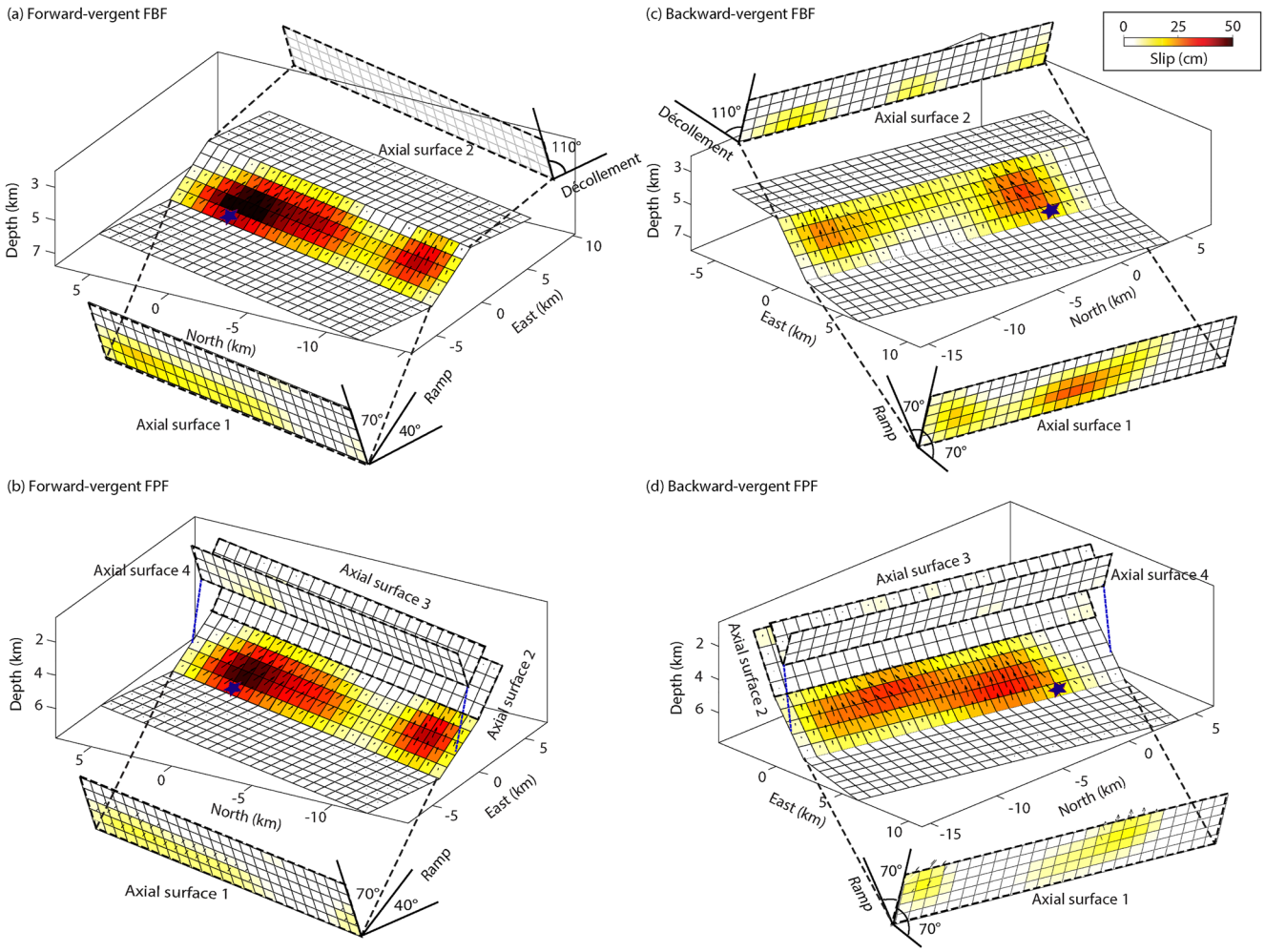

Figure 3. Kinematic models of the Mw 5.7 Dajal earthquake for two-end member fault-related fold geometries and two vergence directions. (a, and c) Forward- and backward-vergent fault-bend fold (FBF) co-seismic slip distribution on the décollement-ramp-décollement system and flexural slip on two axial surfaces. (b and d) Forward- and backward-vergent FPF co-seismic slip distribution on the décollement-ramp system and flexural slip on four active axial surfaces.

(Figure 2a). For the FPF, the model includes slip on the décollement-ramp system and flexural slip on the four active axial surfaces: one aligned with the hinge of the fault bend, two at the top of the fold, and one at the tip of the ramp (Figure 2c). In simple models of folding, flexural slip accommodates the advection of thrusted sediments through the active axial surface as they start or stop climbing the ramp. This localized plastic deformation can be represented by dislocation theory, whereby the nucleus of strain is defined by the unit normal vector $\boldsymbol{n}$ of the axial surface and the direction of long-term motion (Sathiakumar et al., 2020). Even though faults and active axial surfaces are drastically different objects, their short-term effect on displacement and stress in the surrounding elastic medium can be represented by double-couple moment tensors and elastic solutions. The direction of long-term motion along an axial surface is the difference between the long-term velocity vectors in the domains that it separates (Daout, Barbot, et al., 2016; Daout, Jolivet, et al., 2016; Sathiakumar et al., 2020) (Figures 2b and 2d). Assuming no cut-off angle of incoming sediment implies the same slip-rate on the ramp and on the décollement, although with different vector directions. The absolute value of long-term slip rate is not required to determine the direction of long-term relative motion along axial surfaces. The geometry of the active axial surfaces is obtained assuming the conservation of layer thickness, length, and cross-sectional area of the incoming sediment in a balanced cross-section (Suppe, 1983; Suppe & Medwedeff, 1990). Details of the geometry and hodographs of the models are discussed in the Section 2.1 in Supporting Information S1. If folding is entirely coseismic with 40° fault-bends, flexural slip should amount to a fraction of the coseismic slip equal to $2\sin(20°) = 0.68$, corresponding to the closure of the hodograph formed by the relative velocity vectors on the

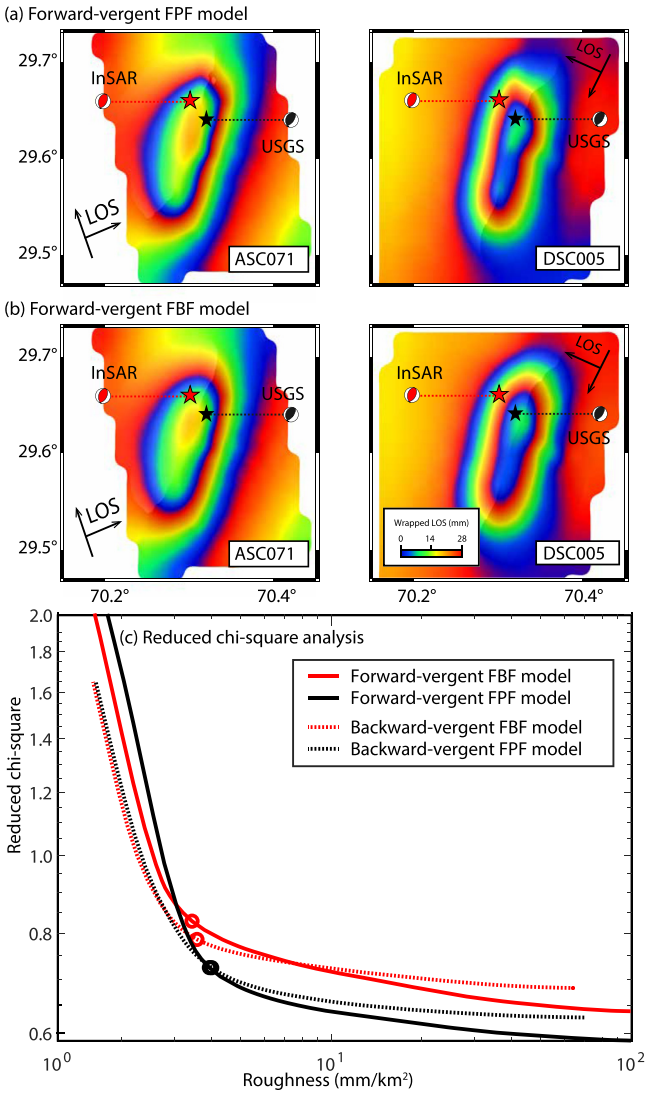

Figure 4. Model comparison. (a) Forward-vergent fault-propagation fold system (FPF) models for ascending and descending interferometric synthetic aperture radar (InSAR) tracks. (b) Forward-vergent fault-bend fold (FBF) models during ascending and descending InSAR tracks. Focal mechanisms based on InSAR (red) or from USGS (black). (c) Tradeoff between data misfit and model roughness (L-curve) for forward- and backward-vergent FBF and FPF models. The black and red color circles show selected smoothing factors for the FBF and FPF models, 0.06, and 0.05, respectively.

décollement, ramp, and axial surface for both forward and backward-vergent models (Figure 2).

We consider the fault-related fold geometries laid out in Figure 2 and the full resolution InSAR observations to estimate the deformation models and corresponding residuals for the forward- and backward-vergent thrusts (Figures S7a–S7r in Supporting Information S1). We model surface deformation due to slip on the ramp and the décollement using analytic solutions (Okada, 1985). For the forward- and backward-vergent FBF models, we determine the distribution of slip on the ramp, two décollements, and the flexural slip over the two axial surfaces through a non-negative least-squares inversion where motion is aligned with the direction of long-term motion (e.g., Barbot et al., 2013; Jónsson et al., 2002). We discretize the model into square patches of 800 m length allowing non-zero along-strike and down-dip slip. We use a L-curve (Aster et al., 2012; Parker, 1994) to resolve the trade-off between misfit and roughness (Figure S8 in Supporting Information S1). The coseismic rupture is much elongated, almost entirely confined to the ramp, with along-strike rupture propagation from north to south, parallel to the BT. Virtually no slip takes place on the shallower or deeper décollements (Figure 3a). The model produces up to 24 cm of flexural slip along the deeper axial surface 1, concentrated near the nucleation area to the north. There is virtually no flexural slip on the shallow axial surface (axial surface 2). There are notable differences for the backward-vergent FBF, which showcases more flexural slip on the axial surfaces than fault slip in the immediate neighborhood of the ramp (Figure 3c).

We now consider the FPF with either a forward- or backward-vergent thrust (Figures 3b and 3d), modeled as a ramp-décollement system with four active axial surfaces. We resolve the spatial distribution of fault and flexural slip using the same approach as above. Both FPF models reveal around 20 cm of flexural slip on axial surface 1, but virtually no flexural slip on surfaces 2, 3, and 4 (Figures 3b and 3d). In the forward-vergent FBF and FPF, the flexural slip follows the pattern of co-seismic slip on the ramp. For the backward-vergent models, flexural slip only occurs near the up-dip tip of the ramp rupture, and coseismic slip is mostly confined on the frontal ramp, with the maximum slip of 50 and 45 cm found at 7.0 km depth respectively (Figures 3b and 3d). The potency density, that is, the stress drop scaled by the rigidity of the host rocks (see Text S3 in Supporting Information S1), is 44 micro-strain, consistent with that of thrust-earthquakes in the region and worldwide (Nanjundiah et al., 2020).

We explore the orientation of the ramp with dip of 30°, 40°, and 50° for all models. The misfit of 40° dip is favored by the data with the lowest root mean square (RMS) for the forward-vergent models (Table S4 in Supporting Information S1). In all cases, the ramp is where most of the blind rupture took place, compatible with our preliminary investigation. In addition, we perform the Akaike Information Criterion (AIC) (Akaike, 1985; Barkat et al., 2022), and reduced-chi-square analyses (Hubbard et al., 2015; Tsang et al., 2016) to evaluate the preferred models (Table S5 in Supporting Information S1). The forward-vergent FPF model shows the lowest RMS, AIC, and reduced-chi-square values with a 40° dipping ramp (Table S5 in Supporting Information S1). We also investigate the depth of the deeper décollment at 6.5, 7.5, 8.5, and 9.5 km (Table S6 in Supporting Information S1). The least systematic residuals correspond to a 7.5 km décollement depth.

The forward-vergent FBF and FPF models (Figures 4a and 4b) explain the observations well, with residuals less than 2.8 mm, and 2.59 mm (Figure S8 and Table S5 in Supporting Information S1). The reduced-chi-square for the forward-vergent FBF and FPF models is 0.82 and 0.72, respectively, even slightly lower for backward-vergent models, with 0.79 and 0.72 (Figure 4c), respectively. However, the forward-vergent models exhibit more internal

consistency than the backward-vergent ones. In the backward-vergent FBF case, there is more flexural slip on the axial surface than fault slip on the ramp at the same along-strike distance, incompatible with fault-related fold kinematics. In the FPF case, the distribution of flexural slip on the deep axial surface is discontinuous. In contrast, the forward-vergent models exhibit features compatible with FBF and FPF kinematics with a distribution of flexural slip on the deep axial surface following the distribution of slip on the ramp and the amount of flexural slip representing 70% of the expected value for coseismic folding. The remaining fraction may occur later in the postseismic period, when folding propagates up-dip of the axial surface through the entire sedimentary stack (Sathiakumar et al., 2020). The 2015 Mw 5.7 Dajal earthquake likely represents the rupture of the frontal section of the BT at the easternmost boundary of the SFT. The rupture can be understood as the seismic activity of the blind, forward-vergent ramp of a FBF or FPF.

3. Discussion

The SFT represents a complex duplex structure with multiple faults and folds that increase in maturity westwards toward the interior of the belt (Khan & Scarselli, 2021; Saif-Ur-Rehman et al., 2019, 2020). North of the Dajal earthquake, where the BT is exposed, the SFT features the Zindapir anticlinorium, characterized by bare Paleocene sediment surrounded by Miocene and younger sediments. The nearby Sakhi Sarwar anticline (Humayon et al., 1991; Saif-Ur-Rehman et al., 2020) shows the development of a fault-bend structure that is less developed and exposes only Miocene and younger sediments. Following this latitudinal progression, we suggest that the Dajal earthquake occurred on the underlying ramp of an even less developed anticlinal structure formed by FPF or FBF buried under the Miocene and younger sediments of the Indus River floodplain (Figure 5). Our interpretation is substantiated by nearby seismic reflection profiles (Humayon et al., 1991; Jadoon, 1995; Saif-Ur-Rehman et al., 2019, 2020) that suggest the presence of a shallow east- and west-dipping décollement at a depth of 7–9 km for fault-related fold structures. The basal décollement and forward-vergent blind ramp may constitute the eastern termination of the SFT, extending the BT farther south and east. The prolongation of the BT is compatible with the overall strike and longitude of the Dajal earthquake ramp. The buried BT may thrust the same sequence of Cretaceous-to-recent sediments that is ubiquitous elsewhere in the SFT. If shortening continues, the fault-related fold will eventually be exposed, as at the Sakhi-Sarwar anticline farther north. It is possible that other thrusts may be found to the west, forming an imbricate structure that can host other earthquakes.

The 2015 Dajal earthquake illuminates the structural control of seismic ruptures and the relationship between faulting and folding at time scales of the seismic cycle. The large aspect ratio (length/width = 6) of the rupture is presumably caused by the termination of the ramp below folded sediments, forcing the rupture to propagate primarily along-strike. If not for the termination of the fault below a synclinal fold, the rupture may have propagated up-dip, producing a larger earthquake with surface breaks. Instead, the rupture concentrates at the base of the ramp, which often constitutes a region of rapid stress accumulation (Sathiakumar & Barbot, 2021). The crustal deformation indicates an apparent synchronicity between coseismic slip and folding of the hanging wall. However, the temporal resolution of radar acquisitions is insufficient to determine whether folding occurred within a few tens of seconds during the earthquake, or within the following hours and days. Truly coseismic folding would imply unstable weakening friction along the bedding planes, corresponding to propagation of flexural slip up-dip of the axial surface at a fraction of seismic shear wave speed. In contrast, flexural slip during the early postseismic period would be compatible with velocity-strengthening friction on the bedding planes that accommodate the deformation. If the spatial distribution of flexural slip—representing only 70% of the maximum expected value—is any indication, the velocity dependence of flexural slip should be strengthening or conditionally stable (Sathiakumar et al., 2020). Otherwise, flexural slip would have propagated farther up-dip as a self-sustaining process. Regardless, folding appears closely synchronized with seismic ruptures, illustrating the strong mechanical coupling between the two modes of brittle deformation at the time scales of the seismic cycle.

Active blind thrusts have shown their seismic potential on many occasions, for example, the 1994 Mw 6.7 Northridge, California (Hudnut et al., 1996), 1999 Mw 7.7 Chi-Chi, Taiwan (A. Lin et al., 2001), and the 2005 Mw 7.6 Kashmir, Pakistan (Powali et al., 2020) earthquakes. Better understanding of crustal dynamics in fold-and-thrust belts is therefore paramount to characterize seismic hazard in regions of active shortening. In the past hundred years, the frontal part of the eastern SFT has not experienced any earthquake of Mw > 6. In contrast, in the Western and Central SFT, several Mw 6.0–6.9 earthquakes occurred in the last decades, including a Mw 6.7 and 6.9 doublet in 1997 in the Sibi Syntaxis (Figure 5a) and Mw 6.4 events in 2008 in the Quetta Syntaxis

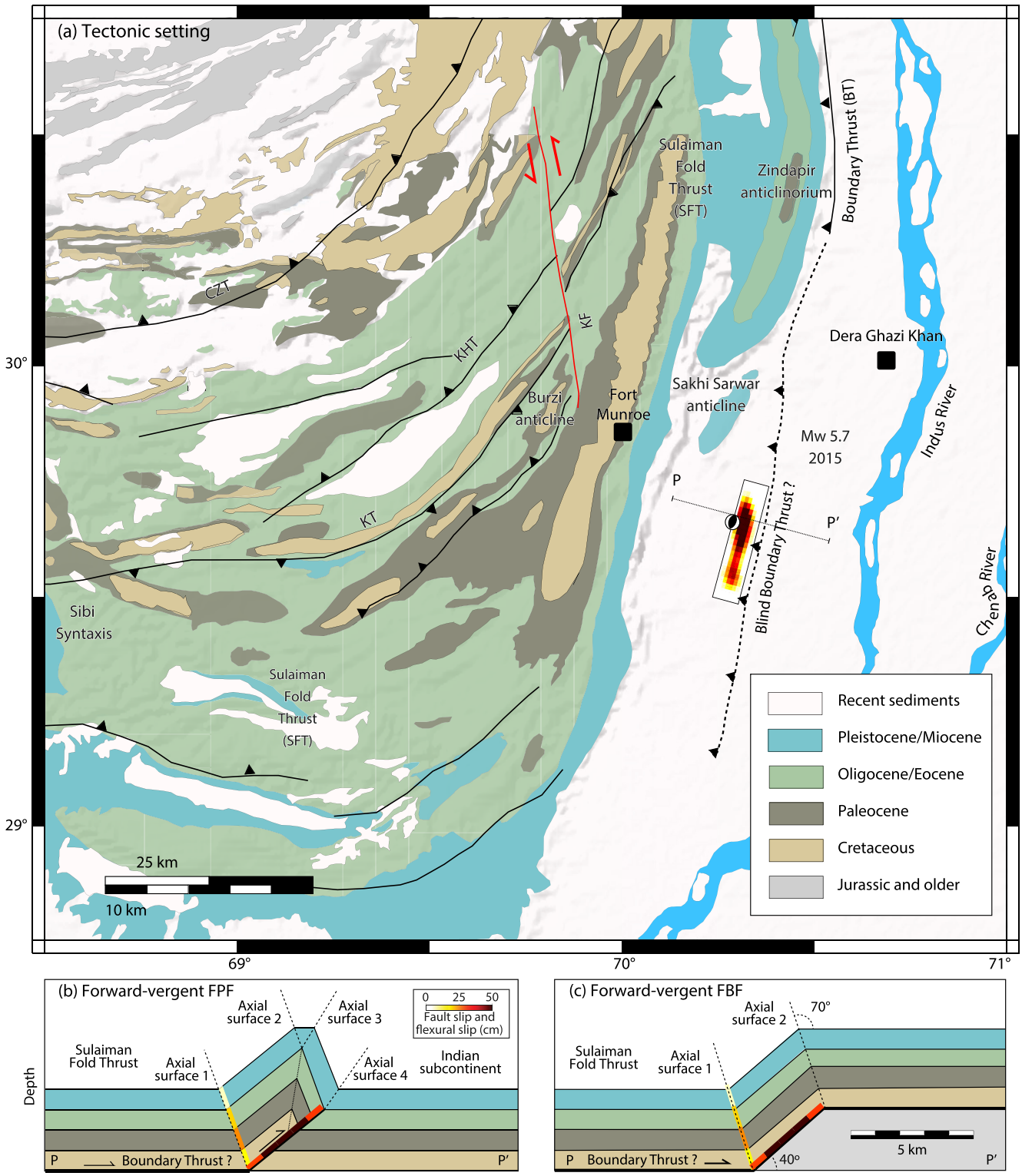

Figure 5. Blind frontal ramp of the Eastern Sulaiman Fold Thrust (SFT). (a) The geological map after Saif-Ur-Rehman et al. (2019). The dashed line with chevron is the proposed extension of the BT south of the Zindapir anticlinorium and the Sakhi Sarwar anticline without surface expression. The ramp is buried under recent sediments from the Indus River flood plain, 30 km east of the Eastern SFT. (b and c) Cross-sections of fault-bend fold and fault-propagation fold (FPF) geometries across the Dajal earthquake epicentral area with a FPF extending from the southern extension of the BT buried under Miocene or younger sediments. The colors indicate the concentration of slip on the ramp and flexural slip along the active axial surface. Vertical exaggeration (x1).

(Figure 1a) (Nissen et al., 2016; Reynolds et al., 2015; Usman & Furuya, 2015). Ultimately, earthquakes accommodate fault slip and the frequency of earthquakes is linked to the long-term fault slip-rate. However, long-term slip-rates vary greatly in space and time in fold-and-thrust belts because shortening occurs both by folding and faulting. During periods of crestal narrowing and uplift, when folds grow mostly vertically, the long-term slip-rate of linked fault sections located up-dip of the fold is momentarily reduced (Suppe, 1983). The long-term slip-rate can be homogeneous along dip during the phase of crustal growth, when a synclinal fold extends forward. As the SFT contains many ramps overlain by folds, the frontal section may experience slower long-term slip-rates, gradually diminishing toward the BT. When shortening is taken up by folding within the belt, the frequency of earthquakes toward the foreland should accordingly decrease, possibly explaining the relative scarcity of earthquakes near the deformation front of the SFT belt in the last hundred years. However, as illustrated by the Dajal earthquake, the propagation of faults into the foreland basin can occur seismically, highlighting the potential seismic hazard of deformation fronts. The interactions of faulting and folding in fold-and-thrust belts therefore exert a control on earthquake processes at the time scales of seismic ruptures, guiding their propagation along strike, and at longer time scales, affecting the average frequency of ruptures.

4. Conclusions

The 2015 Mw 5.7 Dajal, Pakistan earthquake represents the seismic rupture of a frontal blind ramp of the SFT, presumably as the seismic expression of a FBF or FPF. The earthquake illuminates the possible extension of the BT 30 km south of the Zindapir anticlinorium where it breaks the surface, corresponding to the propagation of the SFT some 30 km east into the Miocene and younger sediments of the Indus River floodplain. The earthquake was accompanied by coseismic folding accommodated by flexural slip along an active axial surface. The deformation is captured at the temporal resolution afforded by the radar acquisitions, which includes between 10 and 18 days of potential postseismic deformation. Despite this short period of observation, flexural slip is tantamount to 70% of the expected value for coseismic folding, indicating strong mechanical coupling and synchronicity between faulting and folding at the time scales of the seismic cycle. While the Dajal earthquake demonstrates the seismic potential of the deformation front of fold-and-thrust belts, the folded sediments above the blind ramp exert a strong control on the rupture propagation. Further seismic exploration of fold-and-thrust belts will be crucial to anticipate the location and size of future seismicity in this widespread tectonic setting.

Data Availability Statement

Sentinel-1A data: https://scihub.copernicus.eu/dhus/#/home. SRTM DEM: https://topex.ucsd.edu/gmtsar/demgen/. The line-of-sight displacement and models for the FBF and FPF cases: https://doi.org/10.5281/zenodo.6617118.

Acknowledgments
MTJ acknowledges funding of the PhD through the Maria Zadro legacy to the Trieste University. SB acknowledges funding from NSF number EAR-1848192. CB acknowledges funding from MIUR-PRIN.

References

Akaike, H. (1985). Prediction and entropy. In *Selected papers of hirotugu akaike* (pp. 387–410). Springer.

Ambraseys, N., & Bilham, R. (2003). Earthquakes and associated deformation in northern Baluchistan 1892-2001. *Bulletin of the Seismological Society of America*, *93*(4), 1573–1605. https://doi.org/10.1785/0120020038

Aster, R. C., Borchers, B., & Thurber, C. H. (2012). *Parameter estimation and inverse problems* (2nd ed.). Academic Press.

Bagnardi, M., & Hooper, A. (2018). Inversion of surface deformation data for rapid estimates of source parameters and uncertainties: A Bayesian approach. *Geochemistry, Geophysics, Geosystems*, *19*(7), 2194–2211. https://doi.org/10.1029/2018gc007585

Banks, C., & Warburton, J. (1986). 'Passive-roof'duplex geometry in the frontal structures of the Kirthar and Sulaiman Mountain belts, Pakistan. *Journal of Structural Geology*, *8*(3–4), 229–237. https://doi.org/10.1016/0191-8141(86)90045-3

Barbot, S., Agram, P., & De Michele, M. (2013). Change of apparent segmentation of the San Andreas fault around Parkfield from space geodetic observations across multiple periods. *Journal of Geophysical Research: Solid Earth*, *118*(12), 6311–6327. https://doi.org/10.1002/2013JB010442

Barkat, A., Javed, F., Joe Tan, Y., Ali, A., Tahir Javed, M., Ahmad, N., et al. (2022). 2019 Mw 5.9 mirpur, Pakistan earthquake: Insights from integrating geodetic, seismic, and field observations. *Seismological Society of America*, *93*(4), 2015–2026. https://doi.org/10.1785/0220210322

Bernard, M., Shen-Tu, B., Holt, W., & Davis, D. (2000). Kinematics of active deformation in the Sulaiman Lobe and range, Pakistan. *Journal of Geophysical Research*, *105*(B6), 13253–13279. https://doi.org/10.1029/1999jb900405

Chapple, W. M. (1978). Mechanics of thin-skinned fold-and-thrust belts. *The Geological Society of America Bulletin*, *89*(8), 1189–1198. https://doi.org/10.1130/0016-7606(1978)89<1189:motfb>2.0.co;2

Couples, G. D., Lewis, H., & Tanner, P. G. (1998). Strain partitioning during flexural-slip folding. *Geological Society, London, Special Publications*, *127*(1), 149–165. https://doi.org/10.1144/GSL.SP.1998.127.01.12

Daout, S., Barbot, S., Peltzer, G., Doin, M.-P., Liu, Z., & Jolivet, R. (2016). Constraining the kinematics of metropolitan Los Angeles faults with a slip-partitioning model. *Geophysical Research Letters*, *43*(21). https://doi.org/10.1002/2016GL071061

Daout, S., Jolivet, R., Lasserre, C., Doin, M.-P., Barbot, S., Tapponnier, P., et al. (2016). Along-strike variations of the partitioning of convergence across the Haiyuan fault system detected by InSAR. *Geophysical Journal International*, *205*(1), 536–547. https://doi.org/10.1093/gji/ggw028

Davis, D., Suppe, J., & Dahlen, F. (1983). Mechanics of fold-and-thrust belts and accretionary wedges. *Journal of Geophysical Research*, *88*(B2), 1153–1172. https://doi.org/10.1029/jb088ib02p01153

Davis, T. L., Namson, J., & Yerkes, R. F. (1989). A cross section of the Los Angeles area: Seismically active fold and thrust belt, the 1987 Whittier Narrows earthquake, and earthquake hazard. *Journal of Geophysical Research*, *94*(B7), 9644–9664. https://doi.org/10.1029/JB094iB07p09644

Eakin, D. H., McIntosh, K. D., Van Avendonk, H., Lavier, L., Lester, R., Liu, C.-S., & Lee, C.-S. (2014). Crustal-scale seismic profiles across the Manila subduction zone: The transition from intraoceanic subduction to incipient collision. *Journal of Geophysical Research: Solid Earth*, *119*(1), 1–17. https://doi.org/10.1002/2013JB010395

Fattahi, H., & Amelung, F. (2016). InSAR observations of strain accumulation and fault creep along the Chaman Fault System, Pakistan and Afghanistan. *Geophysical Research Letters*, *43*(16), 8399–8406. https://doi.org/10.1002/2016gl070121

Hubbard, J., Almeida, R., Foster, A., Sapkota, S. N., Bürgi, P., & Tapponnier, P. (2016). Structural segmentation controlled the 2015 Mw 7.8 Gorkha earthquake rupture in Nepal. *Geology*, *44*(8), 639–642. https://doi.org/10.1130/G38077.1

Hubbard, J., Barbot, S., Hill, E. M., & Tapponnier, P. (2015). Coseismic slip on shallow décollement megathrusts: Implications for seismic and tsunami hazard. *Earth-Science Reviews*, *141*, 45–55. https://doi.org/10.1016/j.earscirev.2014.11.003

Hudnut, K. W., Shen, Z., Murray, M., McClusky, S., King, R., Herring, T., et al. (1996). Co-seismic displacements of the 1994 Northridge, California, Earthquake. *Bulletin of the Seismological Society of America*, *86*(1b), S19–S36.

Humayon, M., Lillie, R. J., & Lawrence, R. D. (1991). Structural interpretation of the eastern Sulaiman foldbelt and foredeep, Pakistan. *Tectonics*, *10*(2), 299–324. https://doi.org/10.1029/90tc02133

Jadoon, I. A. (1995). Three dimensional geometry of passive-roof duplex, quaternary transpression, and hydrocarbon traps in the Sulaiman Foreland, Pakistan. *Pakistan Journal of Hydrocarbon Research*, *7*, 9–29.

Johnson, K. M. (2018). Growth of fault-cored anticlines by flexural slip folding: Analysis by boundary element modeling. *Journal of Geophysical Research: Solid Earth*, *123*(3), 2426–2447. https://doi.org/10.1002/2017JB014867

Johnson, K. M., & Johnson, A. M. (2002). Mechanical models of trishear-like folds. *Journal of Structural Geology*, *24*(2), 277–287. https://doi.org/10.1016/S0191-8141(01)00062-1

Jónsson, S., Zebker, H., Segall, P., & Amelung, F. (2002). Fault slip distribution of the 1999 Mw 7.1 Hector Mine, California, earthquake, estimated from satellite radar and GPS measurements. *Bulletin of the Seismological Society of America*, *92*(4), 1377–1389. https://doi.org/10.1785/0120000922

Kaneko, Y., Hamling, I., Van Dissen, R., Motagh, M., & Samsonov, S. (2015). InSAR imaging of displacement on flexural-slip faults triggered by the 2013 Mw 6.6 Lake Grassmere earthquake, central New Zealand. *Geophysical Research Letters*, *42*(3), 781–788. https://doi.org/10.1002/2014GL062767

Kastelic, V., & Carafa, M. M. (2012). Fault slip rates for the active External Dinarides thrust-and-fold belt. *Tectonics*, *31*(3). https://doi.org/10.1029/2011TC003022

Khan, N., & Scarselli, N. (2021). Seismostratigraphic architecture of the Sulaiman Fold-Thrust belt front (Pakistan): Constraints for resource potential of the Cretaceous-Paleogene strata in the east Gondwana fragment. *Journal of Asian Earth Sciences*, *205*, 104598. https://doi.org/10.1016/j.jseaes.2020.104598

Kopp, H., & Kukowski, N. (2003). Backstop geometry and accretionary mechanics of the Sunda margin. *Tectonics*, *22*(6). https://doi.org/10.1029/2002tc001420

Kuo, Y.-T., Ayoub, F., Leprince, S., Chen, Y.-G., Avouac, J.-P., Shyu, J. B. H., et al. (2014). Coseismic thrusting and folding in the 1999 Mw 7.6 Chi-Chi earthquake: A high-resolution approach by aerial photos taken from Tsaotun, central Taiwan. *Journal of Geophysical Research: Solid Earth*, *119*(1), 645–660. https://doi.org/10.1002/2013JB010308

Lai, K.-Y., Chen, Y.-G., Hung, J.-H., Suppe, J., Yue, L.-F., & Chen, Y.-W. (2006). Surface deformation related to kink-folding above an active fault: Evidence from geomorphic features and co-seismic slips. *Quaternary International*, *147*(1), 44–54. https://doi.org/10.1016/j.quaint.2005.09.005

Lavé, J., & Avouac, J.-P. (2000). Active folding of fluvial terraces across the Siwaliks hills, Himalayas of central Nepal. *Journal of Geophysical Research*, *105*(B3), 5735–5770. https://doi.org/10.1029/1999jb900292

Lentas, K., Di Giacomo, D., Harris, J., & Storchak, D. A. (2019). The ISC bulletin as a comprehensive source of earthquake source mechanisms. *Earth System Science Data*, *11*(2), 565–578. https://doi.org/10.5194/essd-11-565-2019

Lin, A., Ouchi, T., Chen, A., & Maruyama, T. (2001). Co-seismic displacements, folding and shortening structures along the Chelungpu surface rupture zone occurred during the 1999 Chi-Chi (Taiwan) earthquake. *Tectonophysics*, *330*(3–4), 225–244. https://doi.org/10.1016/S0040-1951(00)00230-4

Lin, J., & Stein, R. S. (1989). Coseismic folding, earthquake recurrence, and the 1987 source mechanism at Whittier Narrows, Los Angeles Basin, California. *Journal of Geophysical Research*, *94*(B7), 9614–9632. https://doi.org/10.1029/JB094iB07p09614

Mahanjane, E. S., & Franke, D. (2014). The Rovuma Delta deep-water fold-and-thrust belt, offshore Mozambique. *Tectonophysics*, *614*, 91–99. https://doi.org/10.1016/j.tecto.2013.12.017

Muñoz, N., & Charrier, R. (1996). Uplift of the western border of the Altiplano on a west-vergent thrust system, northern Chile. *Journal of South American Earth Sciences*, *9*(3–4), 171–181. https://doi.org/10.1016/0895-9811(96)00004-1

Nabavi, S. T., & Fossen, H. (2021). Fold geometry and folding – a review. *Earth-Science Reviews*, *222*, 103812. https://doi.org/10.1016/j.earscirev.2021.103812

Namson, J., & Davis, T. (1988). Seismically active fold and thrust belt in the San Joaquin Valley, central California. *The Geological Society of America Bulletin*, *100*(2), 257–273. https://doi.org/10.1130/0016-7606(1988)100<0257:safatb>2.3.co;2

Nanjundiah, P., Barbot, S., & Wei, S. (2020). Static source properties of slow and fast earthquakes. *Journal of Geophysical Research: Solid Earth*, *125*(12), e2019JB019028. https://doi.org/10.1029/2019JB019028

Nissen, E., Elliott, J., Sloan, R., Craig, T., Funning, G., Hutko, A., et al. (2016). Limitations of rupture forecasting exposed by instantaneously triggered earthquake doublet. *Nature Geoscience*, *9*(4), 330–336. https://doi.org/10.1038/ngeo2653

Okada, Y. (1985). Surface deformation due to shear and tensile faults in a half-space. *Bulletin of the Seismological Society of America*, *75*(4), 1135–1154. https://doi.org/10.1785/bssa0750041135

Parker, R. L. (1994). *Geophysical inverse theory*. Princeton University Press.

Pezzo, G., Merryman Boncori, J. P., Atzori, S., Antonioli, A., & Salvi, S. (2014). Deformation of the western Indian plate boundary: Insights from differential and multi-aperture InSAR data inversion for the 2008 Baluchistan (Western Pakistan) seismic sequence. *Geophysical Journal International*, *198*(1), 25–39. https://doi.org/10.1093/gji/ggu106

Poblet, J., & Lisle, R. J. (2011). Kinematic evolution and structural styles of fold-and-thrust belts. *Geological Society, London, Special Publications*, *349*(1), 1–24. https://doi.org/10.1144/SP349.1

Powali, D., Sharma, S., Mandal, R., & Mitra, S. (2020). A reappraisal of the 2005 Kashmir (Mw 7.6) earthquake and its aftershocks: Seismotectonics of NW Himalaya. *Tectonophysics*, *789*, 228501. https://doi.org/10.1016/j.tecto.2020.228501

Prevot, R., Hatzfeld, D., Roecker, S., & Molnar, P. (1980). Shallow earthquakes and active tectonics in eastern Afghanistan. *Journal of Geophysical Research*, *85*(B3), 1347–1357. https://doi.org/10.1029/jb085ib03p01347

Price, R. (1981). The Cordilleran foreland thrust and fold belt in the southern Canadian Rocky Mountains. *Geological Society, London, Special Publications*, *9*(1), 427–448. https://doi.org/10.1144/GSL.SP.1981.009.01.39

Qiu, Q., & Barbot, S. (2022). Tsunami excitation in the outer wedge of global subduction zones. *Earth-Science Reviews*, *230*, 104054. https://doi.org/10.1016/j.earscirev.2022.104054

Reynolds, K., Copley, A., & Hussain, E. (2015). Evolution and dynamics of a fold-thrust belt: The Sulaiman range of Pakistan. *Geophysical Journal International*, *201*(2), 683–710. https://doi.org/10.1093/gji/ggv005

Saffer, D. M., & Bekins, B. A. (2002). Hydrologic controls on the morphology and mechanics of accretionary wedges. *Geology*, *30*(3), 271–274. https://doi.org/10.1130/0091-7613(2002)030<0271:hcotma>2.0.co;2

Saif-Ur-Rehman, K. J., Ding, L., Jadoon, I. A., Baral, U., Qasim, M., & Idrees, M. (2019). Interpretation of the eastern Sulaiman fold-and-thrust belt, Pakistan: A passive roof duplex. *Journal of Structural Geology*, *126*, 231–244. https://doi.org/10.1016/j.jsg.2019.06.010

Saif-Ur-Rehman, K. J., Ding, L., Jadoon, I. A., Idrees, M., & Zaib, M. O. (2020). Geometry and development of Zindapir anticlinorium, Sulaiman range, Pakistan. *Journal of Structural Geology*, *131*, 103932. https://doi.org/10.1016/j.jsg.2019.103932

Sandwell, D., Mellors, R., Tong, X., Wei, M., & Wessel, P. (2011). *GMTSAR: An InSAR processing system based on generic mapping tools*. Library – Scripps Digital Collection.

Sathiakumar, S., & Barbot, S. (2021). The stop-start control of seismicity by fault bends along the Main Himalayan Thrust. *Communications Earth & Environment*, *2*(1), 1–11. https://doi.org/10.1038/s43247-021-00153-3

Sathiakumar, S., Barbot, S., & Hubbard, J. (2020). Seismic cycles in fault-bend folds. *Journal of Geophysical Research: Solid Earth*, *125*(8), e2019JB018557. https://doi.org/10.1029/2019JB018557

Sepehr, M., & Cosgrove, J. (2004). Structural framework of the Zagros fold–thrust belt, Iran. *Marine and Petroleum Geology*, *21*(7), 829–843. https://doi.org/10.1016/j.marpetgeo.2003.07.006

Shaw, J. H., Connors, C. D., & Suppe, J. (2005). *Seismic interpretation of contractional fault-related folds: An AAPG seismic atlas* (Vol. 53). American Association of Petroleum Geologists. https://doi.org/10.1306/St531003

Shaw, J. H., Novoa, E., & Connors, C. D. (2004). *Structural controls on growth stratigraphy in contractional fault-related folds*. American Association of Petroleum Geologists.

Shaw, J. H., & Shearer, P. M. (1999). An elusive blind-thrust fault beneath metropolitan Los Angeles. *Science*, *283*(5407), 1516–1518. https://doi.org/10.1126/science.283.5407.1516

Shaw, J. H., & Suppe, J. (1994). Active faulting and growth folding in the eastern Santa Barbara Channel, California. *The Geological Society of America Bulletin*, *106*(5), 607–626. https://doi.org/10.1130/0016-7606(1994)106<0607:afagfi>2.3.co;2

Shaw, J. H., & Suppe, J. (1996). Earthquake hazards of active blind-thrust faults under the central Los Angeles basin, California. *Journal of Geophysical Research*, *101*(B4), 8623–8642. https://doi.org/10.1029/95JB03453

Suppe, J. (1983). Geometry and kinematics of fault-bend folding. *American Journal of Science*, *283*(7), 684–721. https://doi.org/10.2475/ajs.283.7.684

Suppe, J., & Medwedeff, D. A. (1990). Geometry and kinematics of fault-propagation folding. *Eclogae Geologicae Helvetiae*, *83*(3), 409–454.

Szeliga, W., Bilham, R., Kakar, D. M., & Lodi, S. H. (2012). Interseismic strain accumulation along the western boundary of the Indian subcontinent. *Journal of Geophysical Research*, *117*(B8). https://doi.org/10.1029/2011jb008822

Tanner, P. G. (1989). The flexural-slip mechanism. *Journal of Structural Geology*, *11*(6), 635–655. https://doi.org/10.1016/0191-8141(89)90001-1

Tapponnier, P., Lacassin, R., Leloup, P., Scharer, U., Dalai, Z., Haisei, W., et al. (1990). The Ailao Shan/red river metamorphic belt: Tertiary left-lateral shear between Indochina and south China. *Nature*, *343*(6257), 431–437. https://doi.org/10.1038/343431a0

Tsang, L. L., Hill, E. M., Barbot, S., Qiu, Q., Feng, L., Hermawan, I., et al. (2016). Afterslip following the 2007 Mw 8.4 Bengkulu earthquake in Sumatra loaded the 2010 mw 7.8 Mentawai tsunami earthquake rupture zone. *Journal of Geophysical Research: Solid Earth*, *121*(12), 9034–9049. https://doi.org/10.1002/2016jb013432

Tsuji, T., Ito, Y., Kido, M., Osada, Y., Fujimoto, H., Ashi, J., et al. (2011). Potential tsunamigenic faults of the 2011 off the Pacific coast of Tohoku Earthquake. *Earth Planets and Space*, *63*(7), 58–834. https://doi.org/10.5047/eps.2011.05.028

Ul-Hadi, S., Khan, S. D., Owen, L. A., & Khan, A. S. (2013). Geomorphic response to an active transpressive regime: A case study along the Chaman strike-slip fault, western Pakistan. *Earth Surface Processes and Landforms*, *38*(3), 250–264. https://doi.org/10.1002/esp.3272

USGS. (2020). *United States geological Survey, Earthquake Lists, maps, and statistics*. USGS.

Usman, M., & Furuya, M. (2015). Complex faulting in the Quetta Syntaxis: Fault source modeling of the October 28, 2008 earthquake sequence in Baluchistan, Pakistan, based on ALOS/PALSAR InSAR data. *Earth Planets and Space*, *67*(1), 1–11. https://doi.org/10.1186/s40623-015-0303-2

Von Huene, R., Kulm, L., & Miller, J. (1985). Structure of the frontal part of the Andean convergent margin. *Journal of Geophysical Research*, *90*(B7), 5429–5442. https://doi.org/10.1029/JB090iB07p05429

Yue, L., Suppe, J., & Hung, J.-H. (2005). Structural geology of a classic thrust belt earthquake: The 1999 Chi-Chi earthquake Taiwan (M_w 7.6). *Journal of Structural Geology*, *27*(11), 2058–2083. https://doi.org/10.1016/j.jsg.2005.05.020